Deep Mining 2024 – P Andrieux & D Cumming-Potvin (eds)

doi:10.36487/ACG_repo/2465_76

Use of inelastic continuum models to assess mine seismicity levels

Cyrille Séguineau de Préval [a,*], Amélie Ouellet [a], Patrick Andrieux [a]

[a] *A2GC, Canada*

Abstract

Inelastic numerical models are increasingly used to understand seismic data. Yet the stochastic nature of seismic events, the inherent simplification of the rock mass in numerical models and computational limitations make it unrealistic to 'predict' single seismic events. The global seismic response (i.e. seismic events within a given time frame and space frame) can, however, be correlated to numerical model outputs also compiled within a time frame and space frame. A tool is proposed to anticipate, from 3D inelastic continuum modelling results, time periods in the life of mine (LOM) susceptible to generating higher seismicity levels. This is achieved by processing the numerical results against catalogues of recorded seismic events, hence defining a 'seismic response index' (SRI). The SRI must not be considered a prediction tool for seismic events but rather an indication of whether a given mining sequence is likely to trigger an induced seismic response and, if so, how severe. The seismic response associated to historical mining which is used to establish the SRI is quantified based upon an aggregation of source parameters (total energy and local magnitude [ML]) from a collection of seismic events occurring after a stope blast and correlated with various numerical indicators extracted from a mine-scale FLAC3D simulation.

Keywords: *continuum inelastic 3D modelling, seismicity, seismic response, deep mining, life of mine simulation*

1 Introduction

Deep mining operations are increasingly challenged by mining-induced seismicity, which can have serious health and safety consequences. Significant mining-induced seismicity can result in extended re-entry times and operational delays, and ground rehabilitation needs in more severe cases. Hence there is a need to better understand and anticipate site-specific mining-induced seismicity.

Seismic data is already routinely used in mine planning and management. For instance, the location of seismic clusters can help locate and identify specific seismogenic geological structures (Woodward et al. 2017). Real-time analysis of seismic events (frequency and local magnitude [ML]) is also generally part of re-entry protocols (Tierney & Morkel 2017). Finally, more detailed event analysis, such as moment tensor inversion, can provide valuable information on the nature of the event itself, helping bettering understanding of the complex underground rock mass state and seismicity (Westley-Hauta & Meyer 2022). Yet the sole analysis of past and present seismic events is not enough to forecast the seismic activity of a mine as its mining sequence unfolds (Malovichko 2017). While some short-term trends can be forecast from the real-time acquisition of seismic events, they cannot anticipate future seismic activities as they largely depend on the planned activities (development and stope mining).

Numerous efforts are made within the mining industry to relate mine-scale numerical modelling results to seismic activity. The first attempts to use seismic event catalogues with numerical modelling were limited to qualitative calibrations. For example, the location of recorded seismic events can be superimposed on plots of numerically inferred stress in yielded zones (Andrieux et al. 2008). Similarly, the use of the deviatoric

* Corresponding author. Email address: cyrille@a2gc.ca

stress-to-strength ratio ($\mathrm{DSR} = (\sigma_1 - \sigma_3)/\mathrm{UCS}$) has often been seen as a proxy for seismic susceptibility. Cotesta et al. (2014) validated the calibration of numerical simulations by comparing the location of recorded seismic events with the numerical zones where the DSR lies within a certain range. The consideration of the DSR when calibrating numerical models is based on pioneering work on the onset of rock mass damage (Martin 1993). These have established that damage to rock mass starts at a DSR of between 0.3 and 0.5. These qualitative model calibrations can be taken a step further and generalised to a more quantitative calibration, as demonstrated by Kalenchuk (2022).

But at this point these calibrations do not provide anticipation for seismic events. Generally, tools for defining a probability of seismicity fall into two categories: (i) explicit and (ii) implicit seismicity modelling. Explicit seismicity modelling consists of explicitly identifying within a numerical model the location of potential seismic events. Malovichko (2017, 2019) identified potential mechanical weaknesses in mine-scale elastic models by systematically screening through all possible planes of failure, calculating the excess shear stress (ESS) on each plane and identifying surfaces with positive ESS on their planes. These surfaces constitute a set of 'modelled' seismic events. This procedure can be qualitatively calibrated with the recorded seismic events by successively adjusting the parameters required in the ESS calculations and/or changing the in situ stress field.

Alternatively, implicit seismicity modelling does not explicitly model the source mechanisms leading to seismic events. These methodologies use past recorded seismic events to establish a correlation with the numerical simulation of the mining sequence over time. When it is evident that seismicity is triggered along identified faults, Jarufe et al. (2020) model the fault plane (a limit equilibrium strength procedure is used to set up the fault plane parameters) and the plastic displacement field obtained by numerical simulations is integrated along the fault plane to get an equivalent seismic moment. This equivalent seismic moment is further processed, leading to an equivalent distribution of seismic events with the same cumulative seismic moment. A calibration factor (percentage of the fault surface) is used to scale the modelled seismic moments with the measured seismic moments on that fault plane. Ultimately a probability of experiencing seismic events above a given magnitude threshold can be obtained from the modelled distribution of seismic events. For sparser seismicity a promising approach is to track the rate of energy release (RER), a method developed by Beck et al. (2007, 2012). The basic principle is to subdivide the volume of interest into cells and to compare within each cell, at all steps (or frames) of the mine-scale model, the values of the encountered rate of energy release with the number and magnitudes of the recorded seismic events. With this cell method, various probabilities can be established. For instance, one can derive the probability of having a seismic event above a given magnitude when the rate of energy release within a cell exceeds a given dissipated plastic energy level (Beck et al. 2007). The calibration with recorded seismic data also allows the building of correlations between the numerically inferred RER and the recorded moment magnitude (Dehkhoda et al. 2023).

The methodology presented in this paper is based on the fact that the stochastic nature of seismic events, the inherent simplification of the rock mass in numerical models and computational limitations (minimum grid size) make it unrealistic to 'predict' single seismic events or precisely located seismic clusters, even with state-of-the-art continuum models used for mine-scale life-of-mine (LOM) simulations. However, the global seismic response (i.e. seismic events within a given time frame and space frame) can be correlated to numerical model outputs also compiled within a time frame and space frame. Instead of predicting seismicity at a particular location, a proxy for seismicity around the mining front will be sought.

2 Preliminary considerations

Before presenting the details of the seismic response index (SRI) assessment, important underlying concepts and assumptions need to be explicitly laid down.

2.1 Use of continuum modelling

Mining-induced seismic events are the result of a change in the stress-strain state of the rock mass and, in some cases, the presence of a geological discontinuity (or multiple discontinuities) at a small/local and/or large/regional scale. These events often have complex source mechanisms that can involve multiple

lithologies and/or several interacting discontinuities which, in order to be properly modelled, require detailed and accurate input data. This includes the mechanical properties of the lithologies and discontinuities involved, and accurate 3D representations of the relevant contacts or discontinuities (including their location, extent, termination, orientation, thickness and geometry).

Whereas the mechanical properties of the lithologies and their general geometry can be represented reasonably well in a continuum model, it is more difficult to account for discontinuities. Even if the required data were reliably available, current computational limitations can make it difficult to consider (in a mine-scale simulation) discontinuities whose characteristic dimension is smaller than that of the stopes. Still, it could be argued that the rock mass parameters (elastic properties and strength envelope that are the result of a downgrade of the intact rock properties) can be adjusted to already include the effects of small-scale structures.

For large-scale geological structures, one limitation remains: their detailed geometrical features and mechanical properties, the knowledge of which, although required, is generally limited. The necessary data are affected by 'unknown unknowns' – data gaps we are not aware of: for example, the presence of seismic discontinuities not visible in the core or underground which will only be noticed once they start to react seismically. These knowledge gaps can introduce major bias during any attempt to predict future seismicity. Even when the spatial extent of a structure is known (including data from observed seismic clusters), its representation in a numerical model requires, at a minimum, some data such as the friction angle and cohesion. The authors are of the opinion that assuming such inputs without some level of confirmation from some sort of measurement is likely to reduce the confidence associated with deterministic explicit numerical results.

For these reasons, a continuum model (instead of a discontinuum model) is judged suitable for the modelling objective pursued (evaluating the level of seismicity triggered by mining), but with one main constraint. Since structures are not explicitly represented, seismicity cannot be considered on a single event basis but rather as a global response. More precisely, the SRI associated with a given stope blast is defined based upon an aggregation of source parameters from a collection of numerous seismic events occurring after that stope blast.

Consequently, the SRI risk profile must not be taken as the prediction of individual seismic events but rather as an indication of whether the considered mining sequence is likely to trigger a more or less potent level of seismicity. Furthermore, the seismic response is particularly relevant when it is grouped over time periods (such as yearly quarters) or within geographic criteria (a specific mining front, for instance). These time and/or spatial groupings leverage the variance inherent to every correlation.

2.2 Materialisation of seismic events in a continuum model

It is believed that the likelihood of triggering seismic events cannot be solely deduced from the stress states computed in a numerical model: instead, a change in the modelled stress state is a more reliable proxy for the triggering of seismicity. Consequently, any attempt to link seismicity to numerical results should consider the changes in the numerical model before and after the stope excavation, and not only the stress state after excavation. This ties in with the work by Beck et al. (2007), whereby the rate of energy release is considered, and not the energy release itself. Consequently, SRI calculations are based on the difference of various numerical quantities between two successive mining stages (or equilibrium states), as will be discussed later in Section 3.

Numerous research programs have led to a global agreement on the various stages of the failure process for brittle rock. A description is given by Martin in his thesis (1993), from which Figure 1 is extracted.

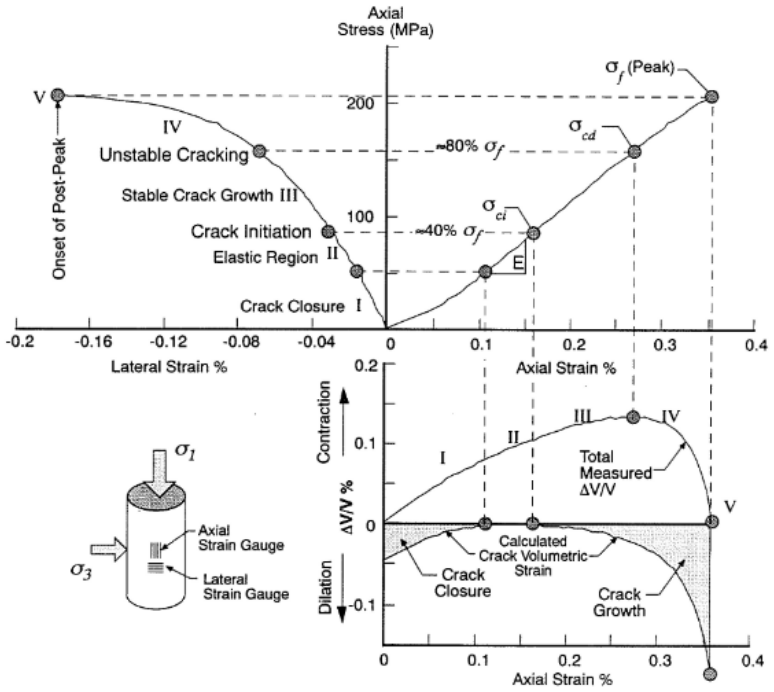

Figure 1 Stress-strain diagram for a single compression test, with the five identified stages in the failure process (I to V). Figure reproduced from Martin (1993)

It is generally accepted that the onset of rock damage occurs at the beginning of the 'stable crack growth' (stage III). This corresponds to a $[\mathrm{DSR} = (\sigma_1 - \sigma_3)/\mathrm{UCS}]$ of between 0.3 and 0.5 (Diederichs 1999; Martin 1993). The measured acoustic events in that stage are independent and randomly located throughout the sample. The next stage is the 'unstable cracking' (stage IV) and it starts at a DSR value of around 0.7 to 0.8. Experience has shown that this threshold is also a limit beyond which the material cannot sustain its integrity under constant load.

It is assumed that this threshold (DSR = 0.7 to 0.8) also marks the limit above which mining-induced seismic events can be recorded by a mine-wide seismic system. Below that DSR value, acoustic emissions have a magnitude lower than about –6 (Sellers et al. 2003), which is below the sensitivity of large-scale seismic arrays at mine sites and makes them unlikely to be detected. Furthermore, Martin (1993) states in his thesis that the seismic events recorded in the experimental mine-by test tunnel and used to establish the crack initiation stress (the beginning of stage III) had magnitudes of between –6 and –4, i.e. still below the sensitivity of mine-wide seismic arrays. Recorded seismic events at mines are thus expected to represent failures in stages IV ('unstable cracking') and V ('onset of post-peak'), as well as post-peak (i.e. after the UCS short-term strength has been reached).

Therefore, a numerical zone with plastic strain should represent a rock mass where the stress has exceeded the crack damage initiation threshold (onset of stage IV) and which could potentially host recordable seismic events. Inversely, intact numerical zones should be within stages I to III which, as stated above, are not generating recordable events (magnitudes within these zones are below –4). Recorded seismic events located in stages I through III of the failure envelope are assumed to be triggered by causes other than mere stress-induced rock matrix failure, and to involve structural discontinuities.

Additional consequences arise from these considerations. Firstly, the aseismic zone near excavations (where no, or very few, seismic events are recorded) should be at (or close to) residual conditions in FLAC3D (ITASCA 2023a). Secondly, the mining-induced high stress front in *FLAC3D* should be located where the seismic events are triggered, or nearby.

3 Establishment of the seismic response index

The seismic response index, referred to as SRI, is meant to anticipate the level of seismicity to be expected as a given mining sequence unfolds. Correlations are first established between the observed seismicity caused by historical stopes ('real' seismic response) and the results of the corresponding numerical simulation steps ('numerical' response). Then these correlations are applied to forward simulation results to estimate future seismic response. The calibration process is schematised in Figure 2. The steps required to establish the SRI are detailed in this section. Examples from an active deep mine are shown throughout the text to illustrate the covered aspects.

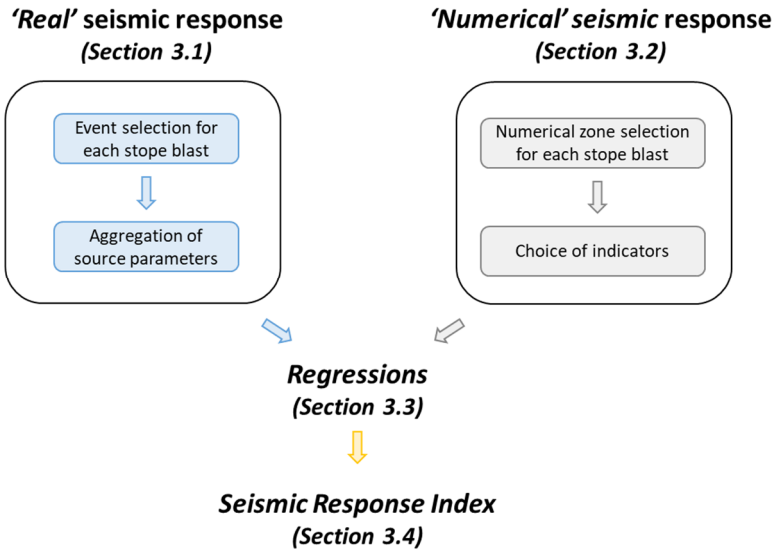

Figure 2 Calibration process for the stress-induced seismic response assessment

3.1 Definition of the 'real' seismic response

3.1.1 Seismic events selection for each stope blast

The 'real' seismic response of a given stope is defined based on the selection of a catalogue of seismic events and a choice of source parameters. Criteria first need to be established to define which seismic events from the catalogue will be considered as triggered by a given stope blast.

In the example case shown in this paper, a seismic event from the catalogue is considered related to a given stope blast if the following two criteria are met: (i) the event is located within 300 m of the stope centroid, and (ii) the event takes place within 11.5 hours of the stope blast time. In other words, the seismic response considered in this example is the immediate and local seismic response. In particular, remote and delayed seismic events are not considered and events that occur on remote fault planes more than 12 hours after a blast are hence excluded from the analysis. This is not seen as a drawback of the methodology but rather as a consequence of the choice made at the beginning of this work. The objective of this specific modelling exercise was to focus on short-term operational challenges (e.g. personnel re-entry procedures and workplace safety).

Another aspect that might be looked at during this stage of the seismic events selection is the underlying mechanism (typically fault-slip versus stress-fracture), when it is available. This has not been considered in the current work.

Stopes are generally extracted in two or three blasts, while numerical mine-scale models usually 'excavate' them in one step. In this case, the events were selected according to the abovementioned criteria for each individual stope blast, and then merged in one single pool. This logic would have been different if the numerical mining sequence considered the individual blasts for each stope.

3.1.2 Aggregation of source parameters

From the selected seismic events taken to be related to a given stope blast, the 'real' seismic response then needs to be characterised based on selected source parameters. These could be ML, the ratio of S-wave energy to P-wave energy (Es/Ep) ratio, total released energy, potency, apparent stress or others.

In the example case shown in this paper, the 'real' seismic response was characterised based on the following two parameters describing the selected events associated with a stope blast: (i) maximum ML (max ML), and (ii) total released energy. These two parameters were selected because they are calculated independently: the moment is based on the Brune model and uses the amplitude of the low frequency displacement spectra, whereas the released energy is proportional to the velocity-squared spectrum integrated across the full frequency domain.

The total released energy is the sum of the energy of all selected events for a stope excavation and max ML is the maximum magnitude of these selected events. Figure 3 shows the total released energy and the max ML for the calibration stopes (95 stopes) used in the example case. The colour scale represents the number of selected events for every stope blast.

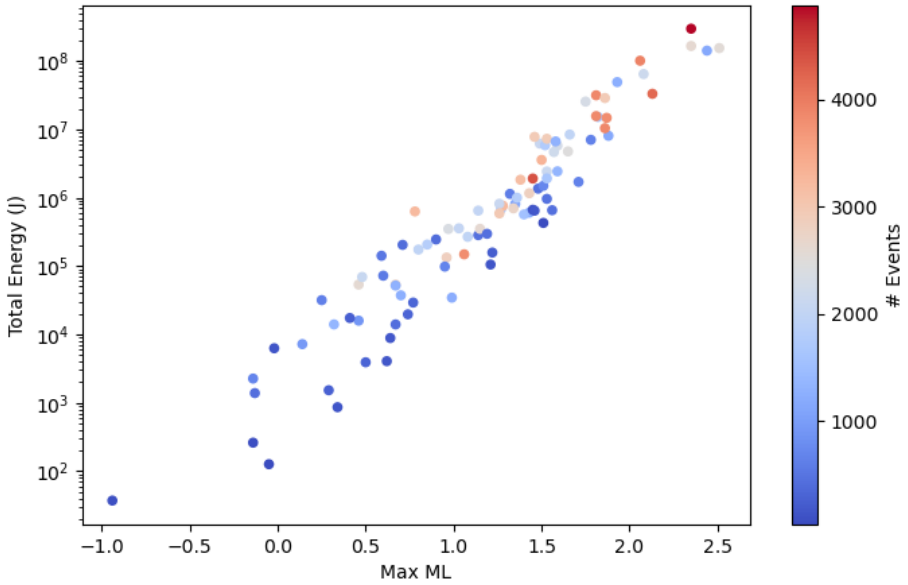

Figure 3 Example of a 'real' seismic response: the relation between the total released energy and the max ML for the selected calibration stopes

It is interesting to note that the total released energy and the max ML present a certain correlation. This reduces the relevance of establishing regressions between numerical indicators and both variables individually. It will be argued later that it is not the max ML that will be forward 'predicted', but whether this value is above or below 1.5 (from a logistic regression instead of a linear regression).

3.2 Definition of the 'numerical' seismic response

3.2.1 Numerical zone selection for each stope

The 'numerical' response of a given stope blast is based on the modelling results for a selection of numerical zones. Similarly to the 'real' seismic response, criteria first need to be established to define which numerical zones in the model will be considered as affected by the simulation of a given stope extraction.

In the example case used in this paper, numerical zones within 100 m of the stope centroid were considered for the collection of numerical quantities to be used in the regressions. Numerical zones containing paste backfill were excluded. It should be noted that for the calibration process, stopes have been mined individually in the simulation.

The distance of 100 m to the stope centroid (instead of 300 m as for the seismic events selection as described in section 3.1.1) was selected for two reasons. Firstly, it was aimed at limiting the amount of numerical data to manipulate. Secondly, because the *FLAC3D* model does not explicitly include structures, the area of influence of a blasted stope observed in the model tends to be more constrained, making it unnecessary to include numerical zones further away than about 100 m from the stope centroid.

3.2.2 Identification of numerical indicators

From the selected numerical zones taken to be related to a given stope excavation, the 'numerical' seismic response then needs to be characterised based on selected indicators. A pool of possible numerical indicators must first be identified. As stated above, preliminary observations have shown that seismic events occur in both intact and yielded numerical zones. This means that the potential variables for regressions (the numerical indicators) should be quantities that apply to both intact and yielded zones.

To account for the plastic behaviour of the rock mass, a first series of quantities based on the energy calculations in *FLAC3D* (ITASCA 2023b) is considered in the example case used in this paper. At each time step, for every numerical zone in the model, the total work variation in the model is computed. Using elastic stress-strain relations, the elastic work is derived from the stress tensor, and the difference before and after the time step leads to the calculation of the elastic work variation. The difference between total work and elastic work is associated with the plastic work. By considering separately the mean and deviatoric parts of the tensors, the shear and volumetric components can be distinguished. The values of those quantities can be stored before and after every stope excavation (or stage) to obtain a differential. The second series of potential quantities is the variation of the softening index (i.e. the relative distance of the strength envelope between the peak strength envelope and the residual strength envelope) caused by the stope excavation. Note that in the example case study, a bilinear Mohr–Coulomb model with strain softening is used.

To account for the elastic behaviour of the rock mass, the deviatoric strength ratio (DSR = $(\sigma_1 - \sigma_3)/\mathrm{UCS}$) is used in our example case. As mentioned, the DSR is a commonly used criterion to match numerical simulations and seismic datasets. Here again it is the variation of the DSR before and after the numerical excavation that will be examined, and not the absolute values. More specifically it is the variation above a certain threshold (taken at 0.3) that is considered in the example case.

At every step, each of the abovementioned quantities is summed over all the selected numerical zones associated with a given stope excavation, thereby providing numerical indicators for each excavated stope (its 'numerical' seismic response) which can then be used as variables for the regressions. For the variation of DSR, a slight adjustment had to be made on the summation: as this variation can be positive or negative depending on the situation (deconfining or progressing stress concentration at the tip of a mined lense around mining front), positive and negative variations are summed separately, resulting in two indicators representing the DSR increase and the DSR decrease, respectively.

Lastly, the authors elected to sum up these indicators within 30 m, 50 m and 100 m spheres around the stope centroid. Preliminary work on the data showed that during the regression process, these three radii could help distinguish between adjacent plastic yielding and elastic behaviour further away.

3.3 Regressions between the seismic parameters and the numerical indicators

From the previous steps, a set of variables on which regressions can be derived is identified. The next step consists of identifying the best regression for each seismic parameter.

A summary of the set of variables identified for the example case is presented in Table 1.

Table 1 Summary of variables available for defining regressions of an example case

Seismic parameters ('Real' seismic response)	Numerical indicators ('Numerical' seismic response)	
	Plastic indicators	Elastic indicators
Total energy release	Plastic work	DSR increase
Maximum ML	Plastic shear work	DSR decrease
	Plastic volumetric work	
	Softening variation	

In this case, two regressions are searched for (one for each seismic parameter), with the following imposed constraints:

- At least one plastic indicator and one elastic indicator should be considered.
- The number of numerical indicators considered should be limited to four. This is meant to keep a certain physical understanding of the regressions without affecting the global performance of the correlations.

Multiple combinations of variables were explored and the two most promising regressions are presented below. Note that logarithms were used for all variables except max ML.

To start, a regression is searched for total energy. The best regression is selected based on the following criteria: (i) correlation coefficient R^2, (ii) visual fit of calibration data and (iii) physical meaning (intuitive).

The two numerical indicators found to best represent the total energy were the plastic shear work within a 100 m radius (PSW_{100}) and the DSR increase, also within a 100 m radius (DSR_{100}). The regression coefficient of this linear regression was found to be 0.27. Isocurves of the linear regression are shown in Figure 4, together with calibration data points. The visual fit was judged satisfying.

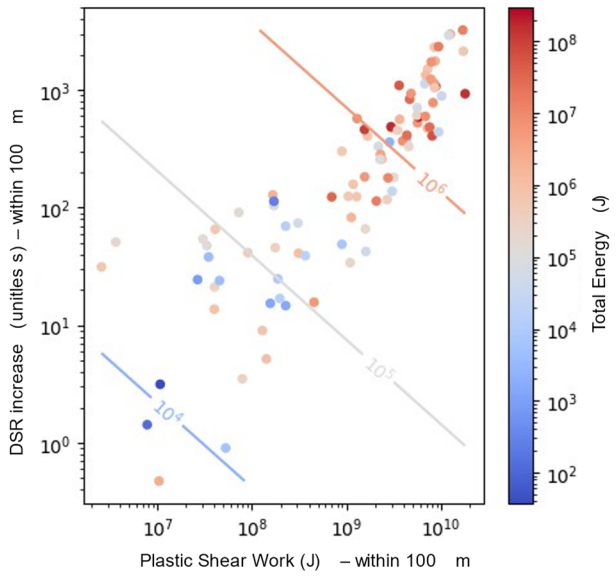

Figure 4 Isocurves of the linear regression for total energy and calibration data points from the example case

For geomechanical applications with high inherent variability, a regression coefficient of 0.27 can be deemed acceptable. However, this relatively low value justifies the search for a second regression on another observed variable (max ML in this case).

Due to the strong correlation observed between the total energy and max ML variables (Figure 3), and because attempts to establish linear regressions with respect to max ML did not result in satisfying regression

coefficients, the max ML dataset was simplified by introducing two classes: Class 0 if max ML is below 1.5, and Class 1 if max ML is above 1.5. A logistic regression was then searched for to fit this max ML class. The 1.5 threshold was selected because it roughly splits the dataset such that one third (1/3) of the datapoints are smaller than the chosen threshold and two third (2/3) higher. A higher value would result in fewer stopes being considered and reduce the performance of the regression.

The identified numerical indicators for the logistic regression that presented the most promising results are listed below:

- Plastic work within 30 m (PW_{30})
- Softening index variation within 30 m (dq_{30})
- DSR increase within 100 m ($\mathrm{DSR}_{inc,100}$)
- DSR decrease within 100 m ($\mathrm{DSR}_{dec,100}$).

A comparison between the max ML class prediction and the real max ML value is shown in Figure 5 for the calibration stopes of the example case. The following is observed:

- Out of 61 stopes that present a max ML value below 1.5, the logistic regression correctly classifies 47 stopes (77%) as having a max ML below 1.5.
- Inversely, out of 33 stopes with a max ML value above 1.5, the logistic regression classifies 18 stopes (55%) to have a max ML above 1.5.

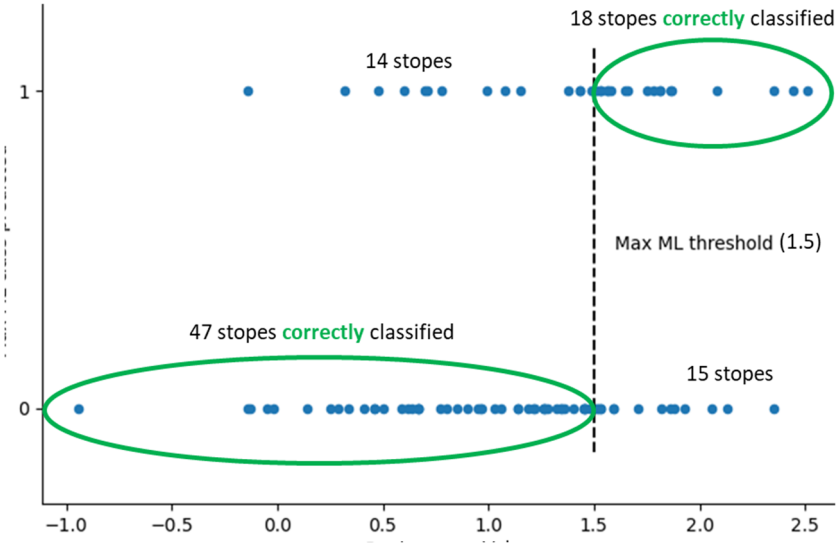

Figure 5 Comparison of the max ML class prediction with the real max ML values of the calibration stopes of the example case

It is concluded that this logistic regression presents an acceptable performance.

3.4 Definition of the seismic response index

The objective of this step is to combine the established regressions (the linear regression for total energy and the logistic regression for max ML) to define an SRI. The SRI is a scalar value, which makes comparisons of the seismic response of two different stopes convenient. The definition of this index is defined hereafter and is specific to the choices of seismic parameters and numerical indicators made beforehand. The example case is used to illustrate the definition of the SRI.

As a start, a scatter plot of the predicted total energy and the max ML class probability obtained from the regressions described in section 3.3 is produced (Figure 6) for the calibration stopes. Despite some variability, a clear trend can be observed.

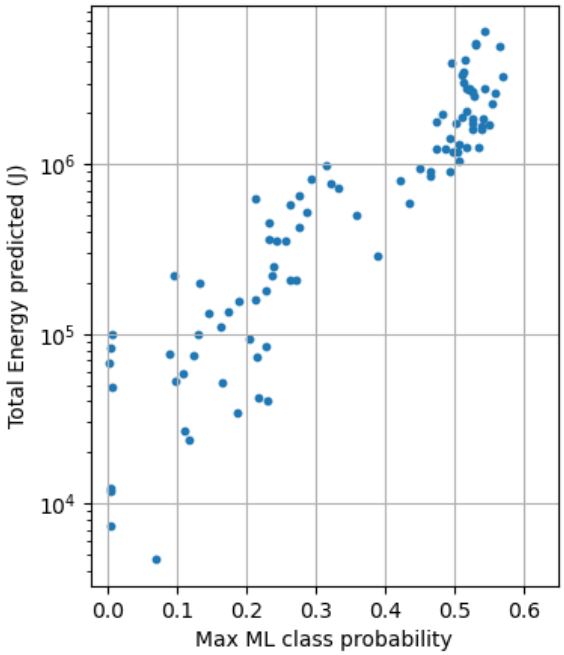

Figure 6 Predicted total energy and Max ML class probability for the calibration stopes of the example case

It should be noted that following some preliminary work, the max ML class probability was used instead of only the max ML class (0 or 1). For example, if a probability of 40% is obtained from the regression for a given stope, a value of 40% is plotted (max ML class probability) instead of assigning a class 0 as is usually done with logistic regressions.

A principal component analysis is then conducted on the results from both predictions to rank all data points with a single scalar value, namely the SRI. The lowest projected data point is assigned an SRI of 0, and the highest projected data point is assigned an SRI of 1. The definition of the SRI is illustrated in Figure 7.

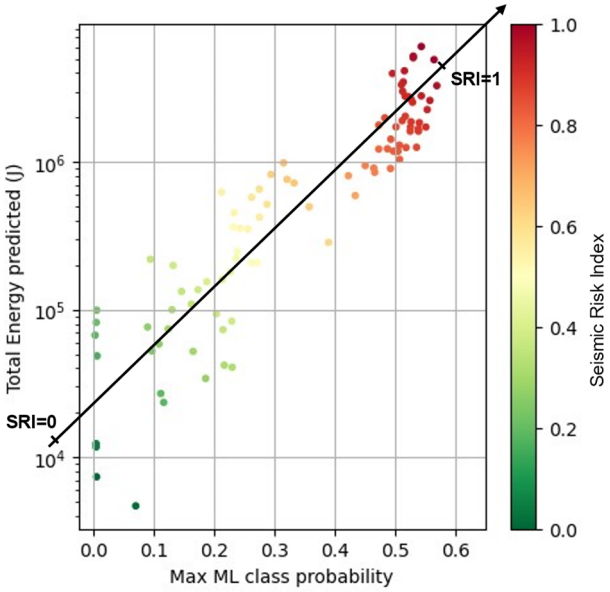

Figure 7 Definition of the seismic response index calibration stopes of the example case study

Figure 8 compares the SRI (obtained from regressions) and the 'real' seismic response (the observed total energy and max ML). In this figure the SRI is represented by the colour scale, while total energy and max ML

are values directly extracted from the seismic events catalogue. Despite some variability, the fit was found to be satisfying (top right data points mostly red, bottom left data points mostly green).

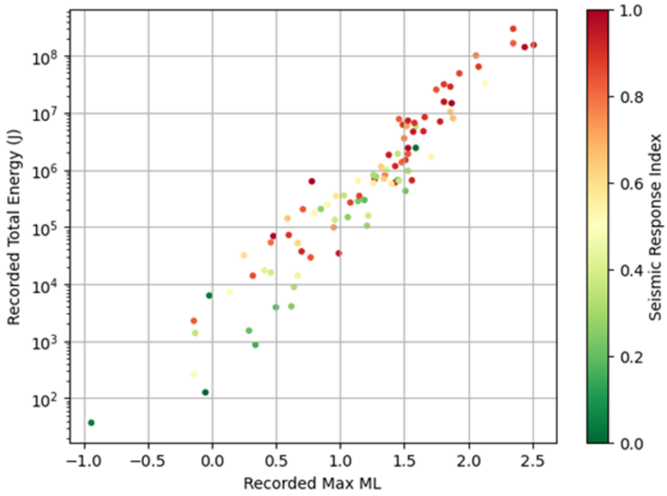

Figure 8 Comparison between the seismic response index and the observed total energy and max ML for the calibration stopes of the example case

It is acknowledged that there are some red data points in the bottom left of the graph: the proposed methodology is still exploratory and there remains room for improvement to refine the SRI. This could be done either by extending the calibration data points used to establish the regressions or by exploring other options of aggregation of source parameters and/or numerical indicators. An aspect that might also explain the variability in the comparison of SRI and observed seismicity is the fact that the source mechanism of the seismic events could not be used during the seismic event selection in the calibration of the SRI. Considering fault-slip induced events, which are often associated with higher magnitudes, while the continuum numerical model ignores known geological structures (and unknown ones) may introduce a bias.

4 Forward simulations

Once regressions between seismic parameters and numerical indicators are established, with a calibrated SRI defined for the historical stopes, this workflow is applied to forward simulations to anticipate future levels of seismicity. Results from the example case study are shown and discussed in this section. The SRI for the future stopes is shown in Figure 9. For reference, the predicted total energy and max ML class probability of the calibration stopes are also shown in this figure.

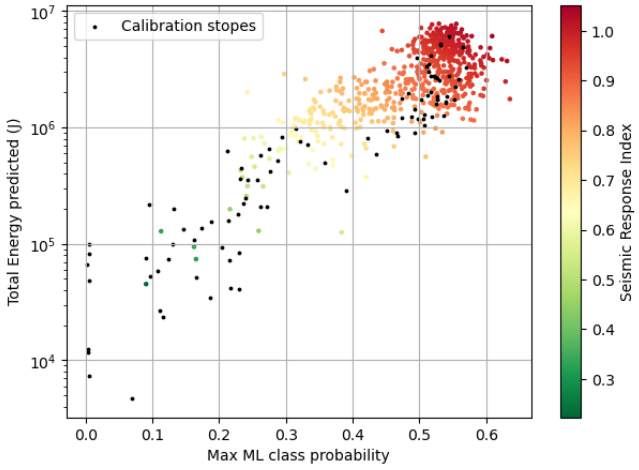

Figure 9 Comparison between the seismic response index for future stopes (colour scale) and the predicted total energy and max ML class probability for the calibration stopes (black) of the example case

At this point it should be reiterated that the SRI is defined based on the calibration stopes. As shown in Figure 7, the lowest calibration data point is assigned an SRI of 0 and the highest calibration data point an SRI of 1. Therefore, future stopes that have an SRI greater than 1.0 are stopes whose SRI is anticipated to be greater than those of the calibration.

As there is an inherent variability in the regressions used the SRI calculations for stopes should be averaged over time periods or regional clusters. In the example case the SRI was averaged over yearly quarters to provide a seismic response risk profile over the life of mine. That risk profile is shown in Figure 10, where the SRI values are averaged for every quarter with a stope volume weighing. Importantly it should be noted that the colour-scale of the SRI has been modified compared to previous figures to be scaled from 0.7 to 1.0. This was done to further highlight differences. Note that this profile only shows the averaged SRI for the forward simulation. Refer to Figure 9 to compare calibration stopes and future stopes on the same graph.

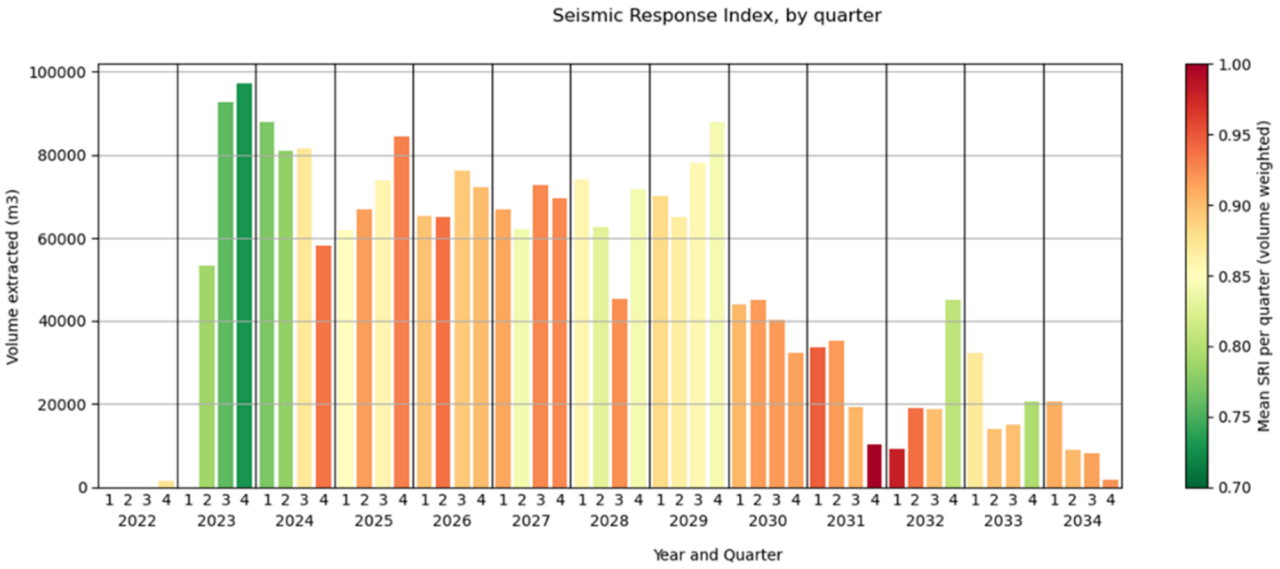

Figure 10 Seismic response index profile by quarter for the example case study

It is observed that some periods are expected to yield important seismic responses, e.g. mid-2025 to 2026 and 2030 to 2032. This information can be used for mine planning, for instance, where specific seismic protocols could be planned to mitigate the seismic hazard.

Additionally, the spatial distribution of the SRI can be visualised by colouring each stope according to its SRI. This allows regional clusters which are likely to trigger seismicity to be readily identified. Here again, this information can be used as a mine planning tool.

5 Conclusion

A concept is put forward to evaluate the global seismic response associated with a given excavation sequence. Numerical model outputs compiled within a time frame and space frame are correlated to seismic parameters also considered within a given time frame and space frame. The obtained SRI is a scalar value intended to provide an appreciation of the seismicity levels associated with future mining. The establishment of the SRI requires a calibration process to be carried out on previously mined stopes. The SRI is meant to be used as a planning tool and the fact that it is a scalar value greatly facilitates its communication.

The case study used throughout this paper to illustrate the SRI methodology contains inherent limitations, such as the sole consideration of local and immediate seismic events and the use of relatively simple regressions to link the numerical indicators to the seismic parameters (total energy and max ML in this case). The authors believe that several improvements can be made. In the case of structurally driven seismicity, numerical outputs exclusively taken at the expected location of a structure or in its vicinity could be used and compared to the seismic events recorded on that structure, even without explicitly including that structure

in the numerical model. One could also broaden the type of numerical indicators used to anticipate the seismic parameters. A promising avenue would be to build upon the concept of excess shear stress.

References

Andrieux, P, Hudyma, M, O'Connor, C, Li, H, Cotesta, L & Brummer, R 2008, 'Calibration of large-scale three-dimensional non-linear numerical models of underground mines using microseismic data', *First International FLAC/DEM Symposium*, Minneapolis.

Beck, D, Levkovitch, V & Simser, B 2012, 'Explicit discontinuum simulation for probabilistic forecasting of fault slip and rock mass seismic potential', in Y Potvin (ed.), *Deep Mining 2012: Proceedings of the Sixth International Seminar on Deep and High Stress Mining*, Australian Centre for Geomechanics, Perth, pp. 373–387, https://doi.org/10.36487/ACG_rep/1201_27_beck

Beck, D, Reusch, F & Arndt, S 2007, 'Estimating the probability of mining-induced seismic events using mine-scale, inelastic numerical models', in Y Potvin (ed.), *Deep Mining 2007: Proceedings of the Fourth International Seminar on Deep and High Stress Mining*, Australian Centre for Geomechanics, Perth, pp. 31–41, https://doi.org/10.36487/ACG_repo/711_2

Cotesta, L, O'Connor, CP, Brummer, RK & Punkkinen, AR 2014, 'Numerical modelling and scientific visualisation – integration of geomechanics into modern mine designs', in M Hudyma & Y Potvin (eds), *Deep Mining 2014: Proceedings of the Seventh International Conference on Deep and High Stress Mining*, Australian Centre for Geomechanics, Perth, pp. 377–394, https://doi.org/10.36487/ACG_rep/1410_25_Cotesta

Dehkhoda, S, Beck, D & Levkovitch, V 2023, 'Numerically simulated rate of energy release and its correlation with measured seismic potency', *Proceedings of the ISRM 15th International Congress on Rock Mechanics and Rock Engineering & 72nd Geomechanics Colloquium – Challenges in Rock Mechanics and Rock Engineering*, International Society for Rock Mechanics, Lisbon.

Diederichs, MS 1999, *Instability of Hard Rockmasses: The Role of Tensile Damage and Relaxation*, PhD thesis, University of Waterloo, Waterloo.

ITASCA 2023a, FLAC3D, computer software, version 9.0, Minneapolis.

ITASCA 2023b, *Itasca Software Guide - FLAC - FLAC Theory and Background - Theoretical Background - Numerical Implementation - Energy Calculations*, Minneapolis.

Jarufe, J, Wesseloo, J, Potvin, Y & Dhanér, C 2020, 'Numerical modelling calculation of probabilistic seismic hazard in cave mining', in R Castro, F Báez & K Suzuki (eds), *MassMin 2020: Proceedings of the Eighth International Conference & Exhibition on Mass Mining*, University of Chile, Santiago, pp. 1225–1234, https://doi.org/10.36487/ACG_repo/2063_90

Kalenchuk, KS 2022, '2019 Canadian Geotechnical Colloquium: Mitigating a fatal flaw in modern geomechanics: understanding uncertainty, applying model calibration, and defying the hubris in numerical modelling', *Canadian Geotechnical Journal*, vol. 59, no. 3, pp. 315–329, https://doi.org/10.1139/cgj-2020-0569

Malovichko, DA 2017, 'Assessment and testing of seismic hazard for planned mining sequences', in J Wesseloo (ed.), *Deep Mining 2017: Proceedings of the Eighth International Conference on Deep and High Stress Mining*, Australian Centre for Geomechanics, Perth, pp. 61–77, https://doi.org/10.36487/ACG_rep/1704_02_Malovichko

Malovichko, DA 2019, 'Calibrating and testing of the forecasts of seismic hazard for planned mining sequences', in J Wesseloo (ed.), *MGR 2019: Proceedings of the First International Conference on Mining Geomechanical Risk*, Australian Centre for Geomechanics, Perth, pp. 245–258, https://doi.org/10.36487/ACG_rep/1905_13_Malovichko

Martin, CD 1993, *The Strength of Massive Lac du Bonnet Granite Around Underground Openings*, PhD thesis, University of Manitoba, Winnipeg.

Sellers, EJ, Kataka, MO & Linzer, LM 2003, 'Source parameters of acoustic emission events and scaling with mining-induced seismicity', *Journal of Geophysical Research: Solid Earth*, vol. 108, no. B9, https://doi.org/https://doi.org/10.1029/2001JB000670

Tierney, SR & Morkel, IG 2017, 'The optimisation and comparison of re-entry assessment methodologies for use in seismically active mines', in J Wesseloo (ed.), *Deep Mining 2017: Proceedings of the Eighth International Conference on Deep and High Stress Mining*, Australian Centre for Geomechanics, Perth, pp. 183–196, https://doi.org/10.36487/ACG_rep/1704_11_Tierney

Westley-Hauta, RL & Meyer, S 2022, 'Characterisation of seismic activity at a kimberlite block caving operation in a complex geological setting in Quebec, Canada', in Y Potvin (ed.), *Caving 2022: Proceedings of the Fifth International Conference on Block and Sublevel Caving*, Australian Centre for Geomechanics, Perth, pp. 1101–1120, https://doi.org/10.36487/ACG_repo/2205_76

Woodward, K, Wesseloo, J & Potvin, Y 2017, 'The spatial and temporal assessment of clustered and time-dependent seismic responses to mining', in J Wesseloo (ed.), *Deep Mining 2017: Proceedings of the Eighth International Conference on Deep and High Stress Mining*, Australian Centre for Geomechanics, Perth, pp. 157–171, https://doi.org/10.36487/ACG_rep/1704_09_Woodward